The Shear-Thinning Elastohydrodynamic Film Thickness of a Two-Component Mixture

Yuchuan Liu

Q. Jane Wang

Center for Surface Engineering and Tribology,
Northwestern University,
2145 Sheridan Road, B224,
Evanston, IL 60208

Ivan Krupka

Martin Hartl

Institute of Machine and Industrial Design,
Faculty of Mechanical Engineering,
Brno University of Technology,
61669 Brno, Czech Republic

Scott Bair[1]

Center for High-Pressure Rheology,
George W. Woodruff School of Mechanical Engineering,
Georgia Institute of Technology,
Atlanta, GA 30332-0405

Lubricant base oils are often blends of different molecular weight cuts to arrive at a specified ambient pressure viscosity and, to improve the temperature-viscosity behavior or to simply increase the viscosity, viscosity-modifying polymer additives are often added to the base oil. This paper investigates the effect of mixture rheology on elastohydrodynamic lubrication (EHL) film thickness using EHL contact measurements and a full numerical analysis for three synthetic lubricants including two single-component lubricants PAO650 and PAO100 and a mixture of these. The pressure and shear dependences of the viscosity of these lubricants were measured with high-pressure viscometers; viscosities were not adjusted to fit experiment. The point contact film thicknesses for these lubricants in pure rolling were measured using a thin-film colorimetric interferometry apparatus. Numerical simulations based on the measured rheology show very good agreement with the measurements of film thickness while the Newtonian prediction is up to twice the measurement. These results validate the use of realistic shear-thinning and pressure-viscosity models, which originate from viscosity measurements. It is conceivable that simulation may provide a means to "engineer" lubricants with the optimum balance of film thickness and friction through intelligent mixing of components.
[DOI: 10.1115/1.2842298]

Keywords: EHL, elastohydrodynamics, rheology, film thickness, shear thinning, non-Newtonian, viscosity

1 Introduction

There has recently been significant progress in obtaining quantitative solutions of the combined Reynolds and elasticity equations for film thickness and even traction in hard elastohydrodynamic lubrication. A Newtonian solution has been generated and experimentally validated [1] for the film thickness in point contact for a reference liquid for which the viscosity and density and film thickness are known accurately. This was possible because the reference liquid, squalane, possesses a large Newtonian limit compared with many liquid lubricants. Generalized Newtonian solutions for film thickness have been obtained and experimentally validated [2] for two dimethyl silicone oils, which severely shear thin at moderate shear stress. Generalized Newtonian solutions for both film thickness and traction have been generated and experimentally validated [3] under combined rolling and sliding conditions for a polyalphaolefin, which gradually shear thins at moderate shear stress. For these simulations, in a significant departure from most previous work, the viscosity was not adjusted to provide the desired result, but instead was obtained from viscometers. These full elastohydrodynamic lubrication (EHL) solutions for low-fragility [4] liquids were validated with experimental measurements of film thickness and traction in relatively low-pressure (~0.5 GPa) steel versus glass contacts operating at low Nahme–Griffith (Brinkman) number. Therefore, it may be concluded that the generalized Newtonian model, along with a precise description of the pressure dependence of the viscosity and of the density, is remarkably accurate [1–3] for film thickness and traction calculations for single-component liquids when the viscosity of the film remains relatively low and thermal softening resulting from viscous heating may be ignored.

The lubricants used in everyday machines are seldom single-component liquids, however. The base oils are often blends of different molecular weight "cuts" to arrive at a specified ambient pressure viscosity. Also, viscosity modifying polymer additives are often blended with the base oil. In particular, the lubricants used in automobiles are usually mixtures. The non-Newtonian behavior of solutions of high-molecular-weight polymers in low-molecular-weight solvents, in shear flow and in extensional flow, has been the subject of much attention in rheology [5]. In addition to shear thinning, normal stress differences in simple shearing, stress overshoot of the steady-state stress at start-up of shearing, and significant increases in elongational viscosity with increasing strain rate are observed in polymer solutions [5]. A most interesting effect is found in the Boger liquids [6]. These liquids display the usual non-Newtonian behaviors, mentioned above, except that the shear viscosity is constant, at least over a range of shear for which the non-Newtonian effects are observed.

A significant contribution to the understanding of the effect of shear thinning on film thickness was made by Dyson and Wilson [7] 40 years ago. They showed that the poor agreement of the classical film thickness formula with experimental measurements on silicone oils was the result of ordinary power-law behavior. A simple Grubin-style inlet analysis has been applied to the EHL film thickness of polymer blends (Ref. [8], for example). To date, a full solution of the combined Reynolds and elasticity equations for film thickness of a mixture has not been offered. This paper addresses the effect of rheology on film thickness for a two-component blend of base oils. Each neat base oil shear thins in the EHL inlet as well. The rheological characterization of a mixture of differing molecular weights is particularly challenging since it is

[1]Corresponding author

Contributed by the Tribology Division of ASME for publication in the JOURNAL OF TRIBOLOGY. Manuscript received September 7, 2007; final manuscript received October 31, 2007; published online March 20, 2008. Assoc. Editor: Michael M. Khonsari.

Table 1 The limiting low-shear viscosity μ in Pa s as a function of pressure for two of the liquids. Similar data for PAO650 at 75°C are reported in Ref. [9]

Pressure p (MPa)	PAO100 50°C	PAO100+PAO650 50°C	PAO100+PAO650 75°C
0.1	0.654	0.913	0.295
25	1.114	1.55	0.455
50	1.79	2.43	0.698
100	4.16	5.63	1.45
150	8.77	11.78	2.86
250	32	43.2	
400	182	235	
600	1560	2080	

Pressure-viscosity coefficients	PAO100	PAO100+PAO650
α_0 (GPa^{-1})	22.5	22.8
α^* (GPa^{-1})	18.2	17.9
α_{film} GPa^{-1}	19.1	18.7

necessary to resolve the viscosity over a broad range of stress; however, with realistic models for the pressure and shear variation of viscosity, simulations may provide a means to "engineer" lubricants, by mixing of components, with the optimum balance of film thickness and friction.

2 Rheological Measurements

The three liquid lubricants which are the subject of this work are all polyalphaolefin (PAO). The PAO650 is a very high viscosity PAO obtained from Mobil Corporation. The PAO100 is one of several 100 cS PAOs that have been studied at Georgia Tech, where all the rheological measurements for this paper were performed, and this particular one was the subject of a previous film thickness study [8]. It possesses an unusual high-molecular-weight "tail" [9] in the molecular weight distribution. An additional experimental liquid was obtained by blending the PAO650 into the PAO100 so that 20% by weight of the mixture is PAO650. All three materials have been described in a previous paper [9] where the pressure and the shear dependences of viscosity were reported.

The limiting low-shear viscosity μ was measured for shear stress $\tau < 10^2$ Pa in falling body viscometers, which may be considered to be accurate to 3%. Additional measurements of μ necessary for the simulation that follows are reported here in Table 1 along with three important pressure-viscosity coefficients [10]:

$$\alpha_0 = \left[\frac{d(\ln \mu)}{dp}\right]_{p=0} \tag{1}$$

$$\alpha^* = \frac{1}{p_{iv}(\infty)} = \left[\int_0^\infty \frac{\mu(p=0)dp}{\mu(p)}\right]^{-1} \tag{2}$$

$$\alpha_{film} = \frac{1-\exp(-3)}{p_{iv}(3/\alpha^*)} \tag{3}$$

Simulation requires an accurate model for the pressure variation of the low-shear viscosity $\mu(p)$ and of the density or volume $V(p)$. The Tait equation

$$\frac{V}{V_0} = 1 - \frac{1}{1+K_0'}\ln\left[1+\frac{p}{K_0}(1+K_0')\right] \tag{4}$$

is considered to be the most accurate isothermal equation of state [11] for high pressures. The Doolittle equation

Table 2 Tait–Doolittle parameters for the experimental liquids at the temperatures of film thickness measurements and calculations

Parameter	PAO100 at 50°C	PAO650 at 75°C	PAO100+PAO650 at 50°C
μ_0 (Pa s)	0.654	1.42	0.913
B	5.209	4.422	5.018
V_∞/V_0	0.6581	0.6694	0.6609
K_0'	11.98	12.82	11.95
K_0 (GPa)	1.312	1.425	1.313

$$\mu = \mu_0 \exp\left[B\frac{V_\infty}{V_0}\left(\frac{1}{\frac{V}{V_0}-\frac{V_\infty}{V_0}} - \frac{1}{1-\frac{V_\infty}{V_0}}\right)\right] \tag{5}$$

is the basis of free-volume models and has the advantage that, when used with the Tait equation, it is capable of representing accurately all of the known viscosity-pressure trends [12] except for the dynamic crossover [4]. The parameters for Eqs. (1) and (2) are listed in Table 2.

The shear dependence of the generalized viscosity $\eta = \tau/\dot{\gamma}$ was measured under pressure for each of the experimental liquids in a previous paper [9]. These data were modeled in the previous paper by a variation of the Ree–Eyring model [13] in which each flow unit was described by a modified Carreau form instead of the inverse hyperbolic form

$$\eta = \mu\sum_{i=1}^{N} f_i\left[1+\left(\frac{\tau}{G_i}\right)^2\right]^{(1-(1/n_i))/2}, \quad \sum_{i=1}^{N} f_i = 1 \tag{6}$$

Equation (6) has the advantage, compared with Ree–Eyring, that the required power-law regimes are naturally incorporated and this results in fewer flow units and the removal of the Ree–Eyring restriction to $N>1$. For the case of a monodisperse liquid, $N=1$. The Vinogradov–Malkin [14] shifting rule has been utilized here; the various G_i are assumed to be constants.

The parameters for Eq. (6) are listed for the three liquids in Table 3. All of the generalized viscosity measurements were obtained in a new pressurized Couette viscometer described in Ref. [15] with the exception that two of the four flow curves used to obtain parameters for PAO650 were generated with an earlier viscometer and different cylinders [16] as well to verify that the results were not dependent on a particular instrument [9]. The working surface dimensions of the Couette cylinder pairs are also listed in Table 3.

In the course of this investigation, it was discovered that the model (6) with parameters from Ref. [9] predicted that the viscosity of the mixture, PAO100+PAO650, at high-shear stress was less than that of the base oil, PAO100. See Fig. 1 where the relative viscosity has been defined as the generalized viscosity of the mixture or the base oil divided by the low-shear viscosity of the mixture. While there is no reason to reject this behavior outright, as molecular alignment of the high-molecular-weight component might induce premature alignment of the low-molecular-weight molecules, it was intuitively disconcerting. Also, these first measurements of shear thinning in the mixture were performed with a Couette cylinder pair of 13.49 mm working diameter with which there was no prior experience except that it reproduced the shear thinning of a NIST non-Newtonian standard at very low stress. This cylinder set was fabricated to better resolve the viscosity over a broad range of shear stress, which is necessary for characterization of mixtures.

As a check, additional measurements were performed on the mixture with the same cylinder pair of 12.67 mm working diameter that was used for the PAO650 measurements. This cylinder pair has also been used to characterize reference liquids [17] and

Table 3 Couette viscometer cylinders and parameters for the modified Ree–Eyring model (6)

Liquid	PAO100	PAO650	PAO100+PAO650	PAO100+PAO650
Data source	Ref. [9]	Ref. [9]	Ref. [9]	New measurements
Cylinder diameter (mm)	9.78	12.67	13.49	12.67
Cylinder length (mm)	2.24	9.67	16.84	9.67
Radial gap (μm)	3.8	5.3	19	5.3
N	2	1	3	3
f_1	0.50	1.00	0.4	0.4
f_2	0.50	—	0.3	0.3
f_3	—	—	0.3	0.3
n_1	0.80	0.74	0.28	0.55
n_2	0.50	—	0.75	0.90
n_3	—	—	0.40	0.40
G_1 (Pa)	1×10^5	3.1×10^4	3.1×10^4	3.1×10^4
G_2 (Pa)	4×10^6	—	1×10^5	1×10^5
G_3 (Pa)	—	—	4×10^6	4×10^6

a NIST non-Newtonian standard [18]. The new data were obtained at 22°C at two pressures, 250 MPa and 300 MPa, and these data are shown in Fig. 1. The new data, obtained with the older cylinder set, show less sensitivity to shear than the original data as represented by the original model parameters. The new data more closely follow the trend for the base oil in Fig. 1 while remaining slightly lower ($\sim$5%) than the base oil.

The effective radial gaps in Table 3 were obtained by measurement on a liquid with known Newtonian viscosity. The 13.49 mm cylinder set has a relatively long working surface in the axial direction and, because its behavior is suspect, the geometry of this set was investigated. Three measurements of the outer diameter of the inner cylinder and the inner diameter of the outer cylinder were made with an outside micrometer ($\pm$2.5 μm) and a hole micrometer ($\pm$5 μm), respectively, positioned near each end and at the middle of the working length. Subtracting the inner cylinder measurements from the outer cylinder measurements, at each of three positions, yielded rather inaccurate measurements of gaps of 8 μm, 8 μm, and 13 μm at the three positions. The anvils of each gauge are 6 mm wide, meaning that large local increases in gap occurring along axial intervals shorter than 6 mm would go undetected. The effective viscous gap is 19 μm, indicating that there are larger local gaps than were directly measured for this cylinder set.

When this large cylinder set was employed for a viscosity measurement, the resulting apparent viscosity was an average of viscosities at the different shear rates occurring along the axis. The averaging of response from varying shear rate regions has the effect of reducing, rather than increasing, the apparent shear dependence of the viscosity, however.

One might speculate that viscous heating at the larger gap regions, which might exist along the axis, may yield thermal softening that would make the viscosity measurement for the larger cylinder set more sensitive to shear than the actual viscosity would be. However, the viscous power is relatively small in these measurements, $\tau\dot{\gamma}<10^8$ W/m^3. For the Nahme–Griffith number Na to be greater than 1, the local gap must be $h>100$ μm and this is unlikely but not impossible. We have no other explanation for the behavior of this cylinder set. The following simulations for the mixture utilize the parameters from the 12.67 mm set only.

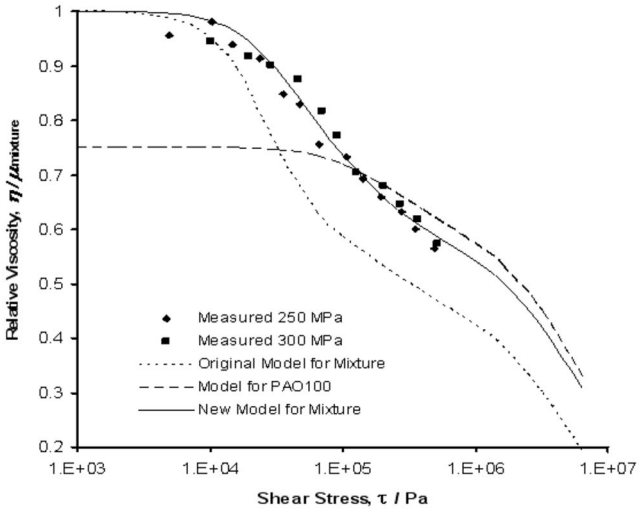

Fig. 1 Comparison of the viscosity function for the base oil, PAO100, and original and new viscosity functions for the mixture, PAO100+PAO650. New viscosity measurements at 22°C generated with the 12.67 mm cylinder set are indicated by points.

3 Tribological Measurements

Film thickness measurements were performed using an experimental apparatus that is fully described in detail elsewhere [19]. In this apparatus, a circular EHL contact is formed between the flat surface of a chromium coated glass disk and a steel ball. The disk is 150 mm in diameter and the ball diameter is 25.4 mm. The root-mean-square surface roughnesses of the balls and disk are about 0.005 μm and 0.002 μm, respectively. The ball is driven by a servomotor and the disk is driven by the ball in nominally pure rolling. The whole contact is enclosed in a thermally isolated, heated chamber, which maintains the test temperature monitored by a small thermocouple located close to the contact inlet. A halogen lamp with filters separating red and green light portion is used as light source and the duochromatic interferograms are recorded with a color video camera attached to a reflected light microscope. Film thickness values are evaluated from the interferograms by thin-film colorimetric interferometry that provides lubricant film thickness measurement down to a few nanometers [20]. The technique is based on colorimetric analysis of duochromatic interferograms using appropriate color matching algorithms and color/film thickness calibration curves. These calibration curves are obtained before each measurement for specific lubricant and contacting bodies. It is believed that the film thickness resolution is approximately 1 nm.

Film thickness experiments were carried out at the load of 30.2 N and lubricant bath temperatures of 50°C (PAO100 and PAO100+PAO650) and 75°C (PAO650). Young's modulus and Poisson's ratio are 81 GPa and 0.208 for glass disk and are 208 GPa and 0.3 for steel ball, yielding reduced Young's modulus of 123.6 GPa. The corresponding Hertzian contact radius and maximum Hertzian pressure are 0.167 mm and 0.517 GPa. Measurements with each lubricant were repeated at least three times with a few hours delay in between to check repeatability at elevated temperatures. Central and minimum film thickness values obtained from these measurements exhibited little variation and all of the repeated data are included in the results presented in this paper.

4 Numerical Simulations

The generalized steady-state Reynolds equation in circular contacts is [3]

$$\frac{\partial}{\partial X}\left(\phi_x \varepsilon \frac{\partial P}{\partial X}\right) + \frac{\partial}{\partial Y}\left(\phi_y \varepsilon \frac{\partial P}{\partial Y}\right) = \frac{\partial(\bar{\rho}H)}{\partial X} \tag{7}$$

where

$$\varepsilon = \left(\frac{a p_H}{12 \bar{u} \mu_0}\right)\left(\frac{\bar{\rho} H^3}{\bar{\mu}}\right) \tag{8}$$

Two flow factors, ϕ_x and ϕ_y, have been introduced to describe the non-Newtonian rheological behavior of a lubricant

$$\phi_x = \frac{12}{p_x}\int_{-1/2}^{+1/2} \xi(\bar{\tau}_a + \xi p_x) f(\bar{\tau}_e) d\xi$$

$$\phi_y = \frac{12}{p_y}\int_{-1/2}^{+1/2} \xi(\bar{\tau}_b + \xi p_y) f(\bar{\tau}_e) d\xi \tag{9}$$

For the lubricant whose viscosity follows the constitutive relationship expressed in Eq. (6), the basic shear-thinning function is defined as

$$f(\bar{\tau}_e) = 1 \Big/ \sum_{i=1}^{N} f_i [1 + (\bar{\tau}_e/\bar{G}_i)^2]^{(n_i-1)/(2n_i)} \tag{10}$$

For smooth surfaces in circular contact, the film thickness is expressed as

$$H = H_0 + \frac{a}{2R}(X^2 + Y^2) + \frac{2p_H}{\pi E'}\int\int_{\Omega} \frac{P(\bar{\xi}, \bar{\zeta})}{\sqrt{(X-\bar{\xi})^2 + (Y-\bar{\zeta})^2}} d\bar{\xi} d\bar{\zeta} \tag{11}$$

The density variation is the reciprocal of the volume variation in Eq. (4),

$$\bar{\rho} = \frac{\rho}{\rho_0} = \frac{V_0}{V} \tag{12}$$

The viscosity variation is based on the Doolittle equation expressed in Eq. (5) and the load balance equation is

$$\int\int_{\Omega} P dX dY = \frac{2\pi}{3} \tag{13}$$

The above EHL equation system was numerically solved based on the numerical method introduced in Ref. [3]. It is noteworthy that the method has been experimentally validated [1] with a reference liquid that is known to be Newtonian within the inlet. A second-order central differencing scheme was used for the left-hand (Poiseuille) side and a second-order backward differencing scheme was used for the right-hand (Couette) side [21] to discretize the Reynolds equation (Eq. (7)) and the DC-FFT algorithm [22] was used to speed up the time-consuming convolution of elastic deformation. In order to calculate the two flow factors, the two shear stresses on the middle layer, $\bar{\tau}_a$ and $\bar{\tau}_b$, can be obtained by applying the following surface speed boundary condition using the Newton–Raphson method.

Table 4 Selection of computational domain according to speed

Computational domain size	Speed (m/s)
$-1.9 < X < 1.1$ and $-1.5 < Y < 1.5$	0.003
$-2.5 < X < 1.5$ and $-2.0 < Y < 2.0$	0.01, 0.03
$-3.5 < X < 1.5$ and $-2.5 < Y < 2.5$	0.1
$-4.5 < X < 1.5$ and $-3.0 < Y < 3.0$	0.3

$$U_s = \int_{-1/2}^{+1/2} (\bar{\tau}_a + \xi p_x) f(\bar{\tau}_e) d\xi$$

$$V_s = \int_{-1/2}^{+1/2} (\bar{\tau}_b + \xi p_y) f(\bar{\tau}_e) d\xi \tag{14}$$

The EHL film thickness experiments described in this paper were obtained for pure rolling. For pure rolling, $\bar{\tau}_a = 0$ and $\bar{\tau}_b = 0$. As a result, the non-Newtonian function defined in Eq. (10) becomes

$$f(\bar{\tau}_e) = 1 \Big/ \sum_{i=1}^{N} f_i [1 + \xi^2 (p_x^2 + p_y^2)/\bar{G}_i^2]^{(n_i-1)/(2n_i)} \tag{15}$$

Accordingly, the two flow factors in Eq. (9) become

$$\phi_x = \phi_y = 12\int_{-1/2}^{+1/2} \xi^2 f(\bar{\tau}_e) d\xi \tag{16}$$

The ten-point Gauss integration algorithm was employed in the above calculation.

Numerical simulations were conducted based on the experimental conditions described in Sec. 3. For pure rolling condition, five entrainment speeds from 0.003 m/s to 0.3 m/s were employed to approximately cover the corresponding speed range in the experiments. Similar to previous simulations for PAO650 in Ref. [3], to avoid numerical starvation for these high viscosity lubricants, a computational domain based on entrainment speed, listed in Table 4, and a fine mesh of 512×512 were employed. The error analysis indicated that the discretization error due to the 512×512 mesh and the second-order backward differential scheme employed in the simulations is smaller than 1%.

Figures 2–4 show the central and minimum film thickness for experiments and simulations for the three lubricants. A linear regression was applied to both the calculated central and minimum film thicknesses and corresponding experimental measurements.

$$\ln(h) = c + b \ln(u) \tag{17}$$

The intercept, slope obtained from regressions, and the relative errors between experiments and simulations are listed in Table 5. In general, the agreements are good. The relative errors for PAO100 are larger than those for the other two liquids; the simulated films are slightly thicker than experiment.

It is observed from Figs. 2–4 that the film thinning due to shear thinning gradually increases as the molecular weight is increased. The more viscous PAO650 possesses higher molecular weight than the PAO100 and its Newtonian limit of 31 kPa is relatively low. As a result, the film thinning effect as presented in Fig. 5 is significant and approaches 50% of the Newtonian prediction as the speed increases. As compared to PAO650, PAO100 exhibits a lower low-shear viscosity but a higher Newtonian limit of 100 kPa and the film thinning approaches 80–90% in Fig. 6. The mixture of 20% PAO650 in PAO100 inherits shear-thinning aspects from both PAO650 and PAO100. As shown in Fig. 1, at

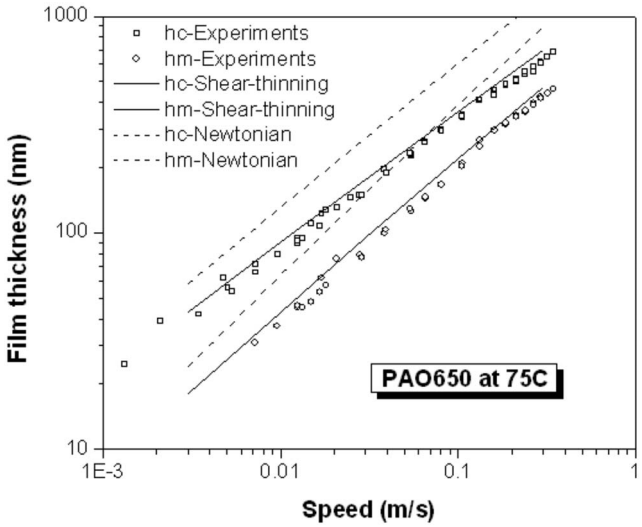

Fig. 2 Comparison of film thickness for PAO650 at 75°C

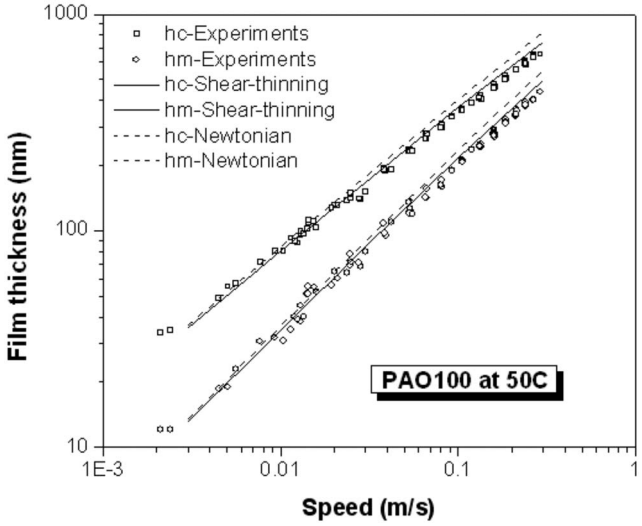

Fig. 3 Comparison of film thickness for PAO100 at 50°C

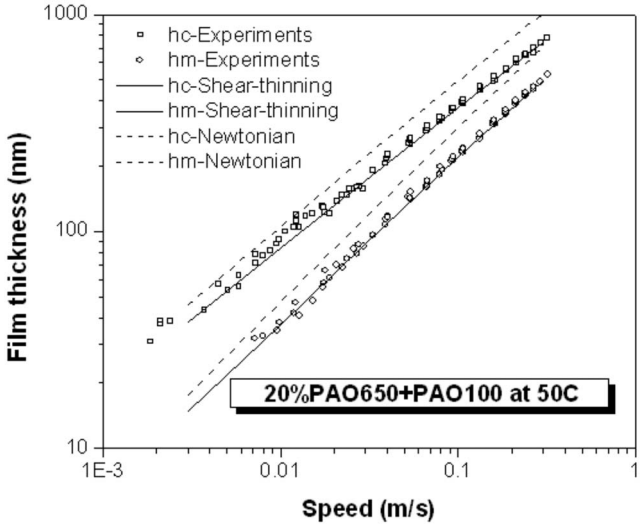

Fig. 4 Comparison of film thickness for 20%PAO650 +PAO100 at 50°C

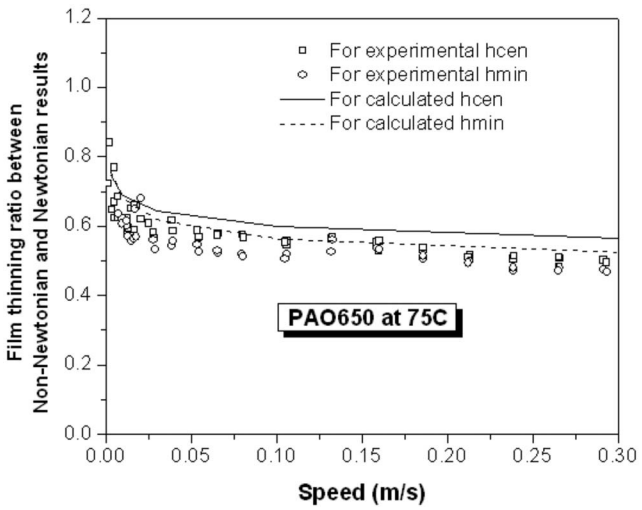

Fig. 5 Film thinning ratio for PAO650 at 75°C

low-shear stress, the mixture exhibits a low Newtonian limit similar to PAO650. At high-shear stress, the shear-thinning effect approaches that for PAO100. It is observed in Fig. 7 that the film thinning effect of the mixture is intermediate to that of the individual components and approaches 70% of the corresponding Newtonian film thickness prediction as the speed increases. As the average molecular weight decreases, as shown in Table 5, the slope of the simulated central film thickness increases from 0.603 to 0.646 to 0.660 and approaches the Newtonian value of 0.67 predicted by the Homrock–Dowson (HD) formula [23].

Dyson and Wilson [7] found that the EHL film thicknesses for polydimethyl silicone lubricants are nearly the same regardless of the low-shear viscosity grade (or, in other words, the molecular weight). Therefore, it would seem to be difficult to increase the film thickness of a silicone lubricant by adding another more viscous silicone. Here, a similar observation can be found in Fig. 8 where the measurement and simulation results for PAO100 and the mixture are displayed together. The improvement in film thickness is very limited although the low-shear viscosity for the mixture is higher than that of the base oil by 25%.

Figure 9 presents the shear stress distribution on the lower surface (that is, the maximum shear stress along the film thickness) for PAO100 and the mixture at different speeds. The difference of

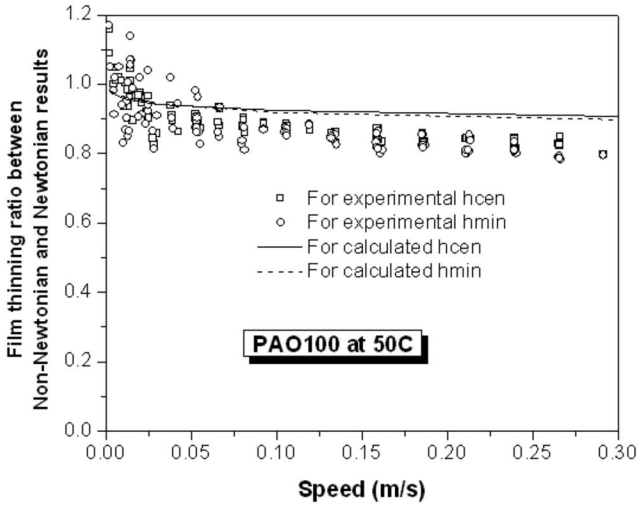

Fig. 6 Film thinning ratio for PAO100 at 50°C

Table 5 Slopes and intercepts regressed from both experimental and simulation results for three PAOs

		Central film thickness			Minimum film thickness		
Lubricants	Parameters	Experiment	Simulation	Error	Experiment	Simulation	Error
PAO650	Slope, b	0.593	0.603	1.7%	0.712	0.705	1%
	Intercept, c	7.163	7.276	1.6%	6.934	7.006	1%
20% PAO650 +PAO100	Slope, b	0.622	0.646	3.7%	0.761	0.765	0.5%
	Intercept, c	7.368	7.402	0.5%	7.158	7.142	0.2%
PAO100	Slope, b	0.623	0.660	5.6%	0.750	0.788	4.8%
	Intercept, c	7.277	7.423	2%	7.018	7.177	2.2%

shear stress between PAO100 and mixture is negligible. The shear stress in the inlet area is closely related to the formation of film thickness. For high-speed case of $u=0.3$ m/s, the maximum shear stress is higher than 1.6 MPa. For very low-speed case of $u=0.003$ m/s, the maximum shear stress is also as high as 0.2 MPa. Due to the symmetry at pure rolling condition, the composite shear stress along the film thickness linearly increases from the zero value at the middle plane of lubricant to the maximum value at two surfaces. The regime of the shear stress smaller than 0.1 MPa, where the main difference was found between PAO100 and the mixture as shown in Fig. 1, is no more than 50% and 6% of the total shear-thinning area, respectively, for $u=0.003$ m/s and $u=0.3$ m/s. Therefore, low-shear viscosity has limited impact on film improvement. In fact, high-shear viscosity is more important than low-shear viscosity in EHL film applications.

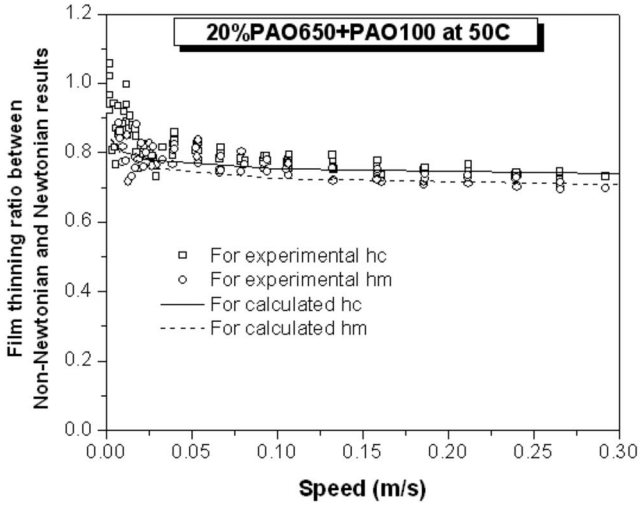

Fig. 7 Film thinning ratio for 20%PAO650+PAO100 at 50°C

5 Conclusions

A realistic EHL simulation in point contact was obtained for two synthetic oils and their mixture using a modified Carreau superposition function for the generalized Newtonian model and the Doolittle–Tait free-volume model for the pressure dependence of viscosity. Viscosities were not adjusted to fit experiment; instead, viscosities were obtained from viscometers. The good agreement between simulation and experiment validates several aspects of the framework for the present modeling system. Measurements of viscosity-pressure response and shear thinning obtained in high-pressure viscometers are essential to an understanding of the mechanisms of film formation. The present EHL numerical code for the generalized Newtonian rheology along with measurements of film thickness obtained in calorimetic interferometry provide necessary insight into film generation. Both experiments and simulations indicate that film thinning becomes significant as the lubricant molecular weight increases. The in-

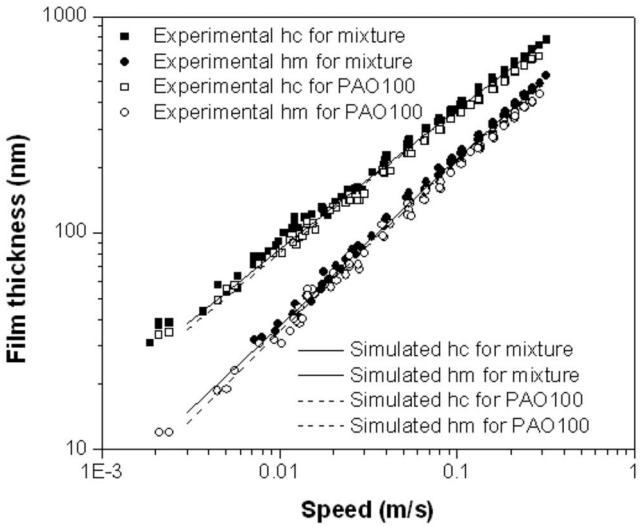

Fig. 8 Comparison of film thickness between single-component PAO100 and mixture 20% PAO650 in PAO100

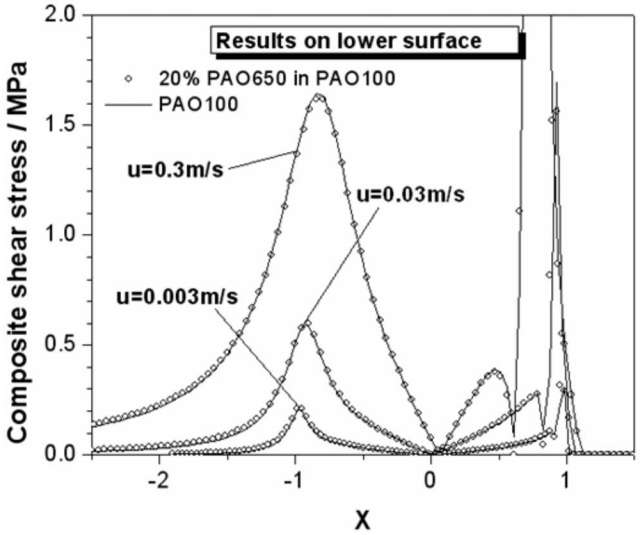

Fig. 9 Shear stress profiles for PAO100 and the mixture at different speeds of $u=0.003$ m/s, 0.03 m/s, and 0.3 m/s

crease in low-shear viscosity afforded by high-molecular-weight thickeners may not translate into the increase in film thickness expected from classical formulas. In EHL applications, the film thickness is determined mainly by high-shear viscosity rather than low-shear viscosity. Simulation may provide a means to "engineer" lubricants with the optimum balance of film thickness and friction through intelligent mixing of components.

Acknowledgment

The experimental results were obtained with the support of the Ministry of Education, Youth and Sports of the Czech Republic (Project No. ME905). Yuchuan Liu and Q. Jane Wang would like to express their gratitude for the support from Office of Naval Research and Department of Energy.

Nomenclature

B = Doolittle parameter
a = Hertzian contact radii, m
D = working diameter, m
E' = reduced Young's modulus of two surfaces, Pa
f_i = ith areal fraction
$f(\bar{\tau}_e)$ = shear-thinning function in the Reynolds equation
$G_i, \bar{G}_i$ = ith modulus, Pa, and dimensionless, $\bar{G}_i = G_i / G_1$
h = film thickness, m
h_c = central film thickness, m
h_m = minimum film thickness, m
K = isothermal bulk modulus, Pa
K_0 = isothermal bulk modulus at $p=0$, Pa
K_0' = pressure rate of change of isothermal bulk modulus at $p=0$
k = thermal conductivity of a liquid, W/m K
N = number of flow units
Na = Nahme–Griffith number, $\mathrm{Na} = \beta \tau^2 h^2 / k\eta$
n_i = ith power-law exponent
p, P = pressure, Pa, and dimensionless, $P = p / p_h$
p_{iv} = isoviscous pressure, $p_{\mathrm{iv}}(p) = \int_0^p \mu(p=0) dp^* / \mu(p^*)$, Pa
p_H = Hertz (maximum) pressure, Pa
p_x, p_y = dimensionless pressure gradients, $p_x = (h/G_1) \times (\partial p / \partial x)$, $p_y = (h/G_1)(\partial p / \partial y)$
R = ball radii, m
$\bar{u}$ = average surface velocity or rolling velocity, m/s
u_i = velocity of surface i, m/s
V = volume at T and p, m^3
V_0 = volume at $p=0$, m^3
V_∞ = occupied volume, m^3
u = velocity in the x direction (generally the rolling direction), m/s
v = velocity in the y direction, m/s
w = velocity in the z direction (generally the cross-film direction), m/s
x, X = coordinate in the direction of surface velocity, m, $X = x/a$
y, Y = coordinate along the surface normal to the surface velocity, m, $Y = y/a$
z, ξ = coordinate across the film, m, $\xi = z/h$
α^* = reciprocal asymptotic isoviscous pressure coefficient $(=1/p_{\mathrm{ai}})$, Pa^{-1}
α_0 = initial pressure-viscosity coefficient, Pa^{-1}
α_{film} = general film-forming pressure-viscosity coefficient, Pa^{-1}
β = temperature-viscosity coefficient, K^{-1}
$\dot{\gamma}$ = shear rate, s^{-1}
η = rate-dependent shear viscosity, Pa s
λ = characteristic time in shear-thinning models, s
$\mu, \bar{\mu}$ = limiting low-shear viscosity, Pa s, and dimensionless $\bar{\mu} = \mu / \mu_0$
μ_0 = low-shear viscosity at $p=0$, Pa s
ν = Poisson's ratio
$\rho, \bar{\rho}$ = mass density, $\mathrm{kg/m}^3$, and dimensionless, $\bar{\rho} = \rho / \rho_0$
ρ_0 = mass density at $p=0$, kg/m
$\tau, \bar{\tau}$ = shear stress, Pa, dimensionless shear stress, $\bar{\tau} = \tau / G_1$
$\bar{\tau}_x, \bar{\tau}_y$ = dimensionless shear stresses in two directions
$\bar{\tau}_e$ = dimensionless combined shear stress, $\bar{\tau}_e = \sqrt{\bar{\tau}_x^2 + \bar{\tau}_y^2}$
$\bar{\tau}_a, \bar{\tau}_b$ = dimensionless shear stresses on the middle layer
ϕ_x, ϕ_y = two flow factors in two directions

References

[1] Liu, Y., Wang, Q. J., Wang, W., Hu, Y., Zhu, D., Krupka, I., and Hartl, M., 2006, "EHL Simulation Using the Free-Volume Viscosity Model," Tribol. Lett., **23**(1), pp. 27–37.
[2] Chapkov, A. D., Bair, S., Cann, P., and Lubrecht, A. A., 2007, "Film Thickness in Point Contacts Under Generalized Newtonian EHL Conditions: Numerical and Experimental Analysis," Tribol. Int., **40**, pp. 1474–1478.
[3] Liu, Y., Wang, Q. J., Bair, S., and Vergne, P., 2007, "A Quantitative Solution for the Full Shear-Thinning EHL Point Contact Problem Including Traction," Tribol. Lett., **28**(2), pp. 171–181.
[4] Bair, S., Roland, M., and Casalini, R., 2007, "Fragility and the Dynamic Crossover in Lubricants," Proc. Inst. Mech. Eng., Part J: J. Eng. Tribol., **221**(7), pp. 801–811.
[5] Tanner, R. I., 2000, *Engineering Rheology*, 2nd ed., Oxford University Press, Oxford, pp. 129–133.
[6] Boger, D. V., 1985, "Model Polymer Fluid Systems," Pure Appl. Chem., **57**(7), pp. 921–930.
[7] Dyson, A., and Wilson, A. R., 1965, "Film Thicknesses in Elastohydrodynamic Lubrication by Silicone Fluids," Proc. Inst. Mech. Eng., **180**, pp. 97–112.
[8] Bair, S., and Qureshi, F., 2003, "The High-Pressure Rheology of Polymer-Oil Solutions," Tribol. Int., **36**(8), pp. 637–645.
[9] Bair, S., Vergne, P., and Querry, M., 2005, "A Unified Shear-Thinning Treatment of Both Film Thickness and Traction in EHD," Tribol. Lett., **18**(2), pp. 145–152.
[10] Bair, S., Liu, Y., and Wang, Q. J., 2006, "The Pressure-Viscosity Coefficient for Newtonian EHL Film Thickness With General Piezoviscous Response," ASME J. Tribol., **123**(3), pp. 624–631.
[11] Hirschfelder, J. O., Curtiss, C. F., and Bird, R. B., 1954, *Molecular Theory of Gases and Liquids*, Wiley, New York, p. 261.
[12] Cook, R. L., Herbst, C. A., and King, H. E., 1993, "High-Pressure Viscosity of Glass Forming Liquids Measured by the Centrifugal Force Diamond Anvil Cell Viscometer," J. Phys. Chem., **97**(10), pp. 2355–2361.
[13] Ree, F. H., Ree, T., and Eyring, H., 1958, "Relaxation Theory of Transport Problems in Condensed Systems," Ind. Eng. Chem., **50**, pp. 1036–1038.
[14] Schurz, J., Vollrath-Rodiger, M., and Krassig, H., 1981, "Rheologische Untersuchungen an Polacrylnitril-Spinnlosungen: Erweiterung HV 6 fur Hohere Temperaturen," Rheol. Acta, **20**, pp. 569–578.
[15] Bair, S., 2007, *High-Pressure Rheology for Quantitative Elastohydrodynamics*, Elsevier Science, Amsterdam, pp. 143–150.
[16] Bair, S., and Winer, W. O., 1993, "A New High-Pressure, High-Shear Stress Viscometer and Results for Lubricants," Tribol. Trans., **36**(4), pp. 721–725.
[17] Bair, S., 2006, "Reference Liquids for Quantitative Elastohydrodynamics: Selection and Rheological Characterization," Tribol. Lett., **22**(2), pp. 197–206.
[18] Bair, S., and Gordon, P., 2006, "Rheological Challenges and Opportunities for EHL," *Proceedings of the IUTAM Symposium on Elastohydrodynamics and Micro-Elastohydrodynamics*, R. W. Snidle and H. P. Evans, eds., Springer-Verlag, Dordrecht, pp. 23–43.
[19] Hartl, M., Krupka, I., Poliscuk, R., and Liska, M., 1999, "An Automatic System for Real-Time Evaluation of EHD Film Thickness and Shape Based on the Colorimetric Interferometry," Tribol. Trans., **42**(2), pp. 303–309.
[20] Hartl, M., Krupka, I., Poliscuk, R., Liska, M., Molimard, J., Querry, M., and Vergne, P., 2001, "Thin Film Colorimetric Interferometry," Tribol. Trans., **44**(2), pp. 270–276.
[21] Liu, Y., Wang, Q. J., Wang, W., Hu, Y., and Zhu, D., 2006, "Effects of Differential Scheme and Mesh Density on EHL Film Thickness in Point Contacts," ASME J. Tribol., **128**(3), pp. 641–653.
[22] Liu, S., Wang, Q., and Liu, G., 2000, "A Versatile Method of Discrete Convolution and FFT (DC-FFT) for Contact Analyses," Wear, **243**(1–2), pp. 101–111.
[23] Hamrock, B. J., and Dowson, D., 1977, "Isothermal Elastohydrodynamic Lubrication of Point Contacts," ASME J. Lubr. Technol., **99**(2), pp. 264–275.